Title
Surface enhanced Raman scattering for detection of Pseudomonas aeruginosa quorum sensing compounds

ISBN
9781628417166

Authors
Thrift, Will
Bhattacharjee, Arunima
Darvishzadeh-Varcheie, Mahsa
et al.

Publication Date
2015-08-31

DOI
10.1117/12.2188806

Surface enhanced Raman scattering for detection of *Pseudomonas aeruginosa* quorum sensing compounds

Will Thrift[a], Arunima Bhattacharjee[a], Mahsa Darvishzadeh-Varcheie[b], Ying Lu[c], Allon Hochbaum[a], Filippo Capolino[b], Katrine Whiteson[c], and Regina Ragan[*a]

[a]Department of Chemical Engineering and Materials Science, University of California, Irvine, Irvine, California 92697, United States; [b]Department of Electrical Engineering and Computer Science, University of California, Irvine, Irvine, California 92697, United States; [c]Department of Molecular Biology and Biochemistry, University of California, Irvine, Irvine, California 92697, United States

ABSTRACT

Pseudomonas aeruginosa (PA), a biofilm forming bacterium, commonly affects cystic fibrosis, burn victims, and immunocompromised patients. PA produces pyocyanin, an aromatic, redox active, secondary metabolite as part of its quorum sensing signaling system activated during biofilm formation. Surface enhanced Raman scattering (SERS) sensors composed of Au nanospheres chemically assembled into clusters on diblock copolymer templates were fabricated and the ability to detect pyocyanin to monitor biofilm formation was investigated. Electromagnetic full wave simulations of clusters observed in scanning electron microcopy images show that the localized surface plasmon resonance wavelength is 696 nm for a dimer with a gap spacing of 1 nm in an average dielectric environment of the polymer and analyte; the local electric field enhancement is on the order of 400 at resonance, relative to free space. SERS data acquired at 785 nm excitation from a monolayer of benzenethiol on fabricated samples was compared with Raman data of pure benzenethiol and enhancement factors as large as 8×10^9 were calculated that are consistent with simulated field enhancements. Using this system, the limit of detection of pyocyanin in pure gradients was determined to be 10 parts per billion. In SERS data of the supernatant from the time dependent growth of PA shaking cultures, pyocyanin vibrational modes were clearly observable during the logarithmic growth phase corresponding to activation of genes related to biofilm formation. These results pave the way for the use of SERS sensors for the early detection of biofilm formation, leading to reduced healthcare costs and better patient outcomes.

Keywords: Colloids, self-assembly, surface enhanced Raman scattering, plasmonics, biofilms, metabolomics, quorum sensing, biosensor

1. INTRODUCTION

Biofilms, cellular aggregates embedded within an extracellular polymeric substance (EPS), account for an estimated 80% of all infection,[1] and commonly contaminate medical devices.[2] Bacterial biofilms are able to survive exposure to antibiotic treatments in part because the EPS reduces diffusion into the center of the biofilm masses, leading to lower exposure to the drug.[3] Bacteria that aggregate into a biofilm also express different phenotypes compared to their free floating, planktonic counterparts[4] and often exhibit resistance mechanisms such as efflux pumps, which specifically pump out antibacterial molecules.[5] *Pseudomonas aeruginosa* (PA) is an opportunistic, biofilm-forming pathogen associated with lung infections in cystic fibrosis and in indwelling device infections.[6] Individuals with the genetic disorder cystic fibrosis (CF) are particularly at risk of biofilm infection because they lack mucociliary clearance mechanisms in the lung epithelia, due to mutations in the CF transmembrane conductance regulator (CFTR) protein.[7,8] Dysfunctional CFTR protein prevents clearance of bacteria entering the lung, enabling biofilm formation.[9,10] PA establishes a chronic infection in CF patients, developing a biofilm with an associated EPS.[11] Prior to chronic infection is the intermittent colonization phase where high doses of antibiotics are used for extended periods of time[12] until the chronic infection eventually forms.[13,14] These conditions have led to the evolution of antibiotic resistant PA which is a serious danger to those at risk of PA infection.[15]

In order for a biofilm to form, members of the population interact with one another via signaling molecules or by trading metabolites, a process known as quorum sensing (QS).[16,17] These signals trigger the conversion of planktonic

Biosensing and Nanomedicine VIII, edited by Hooman Mohseni, Massoud H. Agahi, Manijeh Razeghi,
Proc. of SPIE Vol. 9550, 95500B · © 2015 SPIE · CCC code: 0277-786X/15/$18 · doi: 10.1117/12.2188806

cells into biofilm cells by altering the phenotypes expressed by the cells.[4] The expressed genes aggregate the cells and start the production of EPS and QS signaling molecules. The process of QS causes specific cells to produce metabolites so that a division of labor is exhibited that proves advantageous for these biofilm forming cells.[18] The success of the consortia then becomes dependent on the efficacy of regulating this QS process in order to produce dedicated molecular signaling for each task. Among the many virulence factors and QS compounds that PA produces is pyocyanin[19]. Pyocyanin is a blue green redox active secondary metabolite that is produced by PA which can act as a terminal signaling factor in the QS process. In the presence of oxygen, phenazines such as pyocyanin can generate reactive oxygen species that are toxic to neighboring bacterial or human cells in an infection, while in low oxygen conditions, phenazines can act as an alternative electron receptor, enabling respiration in dense biofilms with low oxygen conditions.[20] Pyocyanin can be detected in PA wound infections and the lungs of infected CF patients using high performance liquid chromatography (HPLC).[21]

Unfortunately HPLC is expensive, time consuming, and requires skilled laborers to use. Optical spectroscopy, such as surface plasmon resonance, and color changes are increasingly used for biomolecule detection.[22] An alternative method is Raman scattering, a label free detection method that produces "molecular fingerprints" composed of the spectrum of the different vibrational frequencies produced when light inelastically scatters with molecules.[23] The Raman scattering cross section is typically on the order of 10^{-6} cm^{-1} per unit volume (cm^{-3}) or 10^{-32} cm^2 for a molecule with length of 1.5 nm[24] and this high limit of detection is not sufficient for diagnostic applications. Surface enhanced Raman scattering (SERS) spectroscopy can have detection limits reaching a single molecule due to enhancements of the local electric field due to nanostructures.[25,26] On a SERS active surface, incoming field light excites the plasmon resonance of nanostructures that generate high intensity fields.[27] As a near field phenomenon, the plasmon modes are not diffraction limited and the electric field is concentrated locally in so called hotspots. Importantly, the a SERS surface serves to enhance the incident electric field, $|\vec{E}|$ that excite molecules as well as the the Raman scattered intensity from molecules in the vicinity of hotspots. In summary the SERS surface acts as nano antennas that enhance the incoming and scattered field compared to a case without SERS active nanostructures with a proportionally of $|\vec{E}|^4$.[28] Engineering hot spots has been heavily pursued since the first measurement of enhanced Raman scattering intensity at roughened electrodes, where simple roughened silver electrode[29] can provide a SERS enhancement factor (EF) of 10^5.[30]

Molecular detection via SERS has heavily benefited from advances in nanofabrication technology as hotspot intensity increases with decreased gap spacing in nanostructures.[31 32] For example, the enhanced electric field intensity, $|\vec{E}|^2$, in the gap region is reported to reach values larger than 10^3 when the gap size in a Au bowtie nanoantenna decreases to values less than 20nm.[33,34] Top-down, planar lithographic approaches such as photolithography, electron beam lithography [35], and ion beam lithography,[36] achieve a variety of nanoscale patterns but are essentially too expensive for medical diagnostic applications. In addition, while gap spacings below 10 nm are desirable for SERS applications, as they yield increasing large signal enhancements with decreasing gap spacing up to the quantum tunneling limit,[37–39] they are extremely difficult to produce with top down methods such as electron beam lithography.[40] In this work, we utilize chemical self-assembly to drive Au nanospheres into clusters with approximately 1 nm separation distances. Chemical self-assembly permits the inexpensive production of large scale (> 1 cm^2) nanostructures with relatively uniform and high single enhancements SERS substrates. SERS sensors have demonstrated capacity for clinical applications with reports of ng/ml limits of detection for pharmaceutical opioids,[41] selectivity of various influenza viruses,[42] part per trillion detection limits of cancer biomarkers,[43] and part per trillion detection limits of milk contaminants.[44] Low cost fabrication of these sensors with low detection limits will have significant impact for medical diagnostic applications including clinical sensing of pyocyanin that has the potential to reduce the cost of healthcare for chronically ill patients, and in the quantification of QS for understanding, and eventually preventing, biofilm formation.

2. MATERIALS AND METHODS

2.1 Materials

Random copolymer Poly(styrene-co-methyl methacrylate)-α-Hydroxyl-ω-tempo moiety (PS-r-PMMA) (M_n = 7,400, 59.6% PS), diblock copolymer poly(styrene-*b*-methyl methacrylate) (PS-*b*-PMMA) diblock copolymer PS-*b*-PMMA with M_n = 170-*b*-144 kg mol^{-1} forming lamellar template) were purchased from Polymer Source, Inc. (Dorval, Canada). Gold nanospheres with a diameter of 40 nm and with lipoic acid functionalization were purchased from Nanocomposix (San Diego, CA). Si(001) wafers with resistivity of 0.001-0.004 ohm-cm were purchased from Virginia

Semiconductor (Frederickburg, VA). Sodium citrate, sodium hydroxide (NaOH), and hydrofluoric acid (HF) were purchased from Fisher Scientific (Pittsburgh, PA). 2-(*N*-morpholino)ethanesulfonic acid (MES) 0.1M buffer, 1-ethyl-3-[3-dimethylaminopropyl] carbodiimide hydrochloride (EDC), and N-hydroxy sulfosuccinimide (S-NHS) were purchased from Pierce (Rockford, IL). Dimethyl sulfoxide (DMSO), ethylenediamine, benzenethiol, pyocyanin, toluene, ethanol, isopropanol (IPA), and 52-mesh Pt gauze foil were all purchased from Sigma Aldrich (St. Louis, MO). Nanopure deionized water (DI) (18.2 MΩ cm^{-1}) was obtained from a Milli-Q Millipore System.

2.2 Nanosensor Fabrication

Template Preparation: Diblock copolymer templates on Si(001) substrates were used as a self-assembled template for chemical assembly of Au nanospheres. A solution of 1 wt% (PS-r-PMMA) random copolymer, in toluene, was deposited onto a clean Si wafer by spin coating at 3000 rpm for 45 s. After spin coating, a PS-r-PMMA brush layer was annealed for 72 hours in low vacuum at 170° C. PS-r-PMMA/Si was then cleaned by rinsing with toluene while spin coating at 3000 rpm in order to remove unbound polymer. Solutions of 1 wt% PS-b-PMMA (PS/PMMA =170 kg mol^{-1} / 144 kg mol^{-1}) in toluene is applied onto the PS-r-PMMA coated wafer at 5000 rpm for 45s; afterward the sample was annealed for 48 hours at 170° C. The PMMA regions of the template were functionalized with amine surface end groups by immersing the whole sample in ethylenediamine in DMSO (2% v/v) for 5 minutes. Additional details can be found here.[45–47]

Nanosphere Functionalization: Au nanospheres with 40 nm diameter were prepared for chemical attachment by centrifuging 0.05 mg/mL solution of nanospheres at 1.1g for 25 minutes to resuspend at triple the initial nanosphere concentration. Chemical attachment of Au nanospheres to PMMA regions on PS-b-PMMA was performed using a chemical crosslinker EDC/S-NHS that was added to the aqueous lipoic acid functionalized colloidal solution. The concentration of EDC and S-NHS in a 0.1 M MES buffer, used were 8 mM and 20 mM, respectively. Addition of crosslinker to aqueous lipoic acid functionalized colloidal solution occurred immediately before exposure to PS-b-PMMA surfaces in order to minimize nanosphere aggregation in solution.

Cluster formation of Au nanospheres on PMMA: Lipoic functionalized Au nanospheres in colloidal solution were selectively attached to ethylenediamine functionalized PMMA domains via electrophoretic deposition (EPD). The ethylenediamine treated PS-*b*-PMMA template on Si was suspended vertically and parallel to a Pt mesh electrode in a 10 mL beaker, serving as the anode. The beaker was then filled with 3 mL of the colloidal Au nanosphere solution, 70 µL of EDC solution, and 70 µL of S-NHS solution. A BK Precision 1621a DC Regulated Power Supply was used to apply a voltage of 1.2 V across a distance of 1 cm for ten minutes. This process was then repeated with 3 mL of the lipoic acid functionalized Au nanosphere solution, 45 µL of EDC solution, and 45 µL of S-NHS solution. Samples were then rinsed with IPA and dried under nitrogen.

2.3 Bacterial cell culture and supernatant preparation

Pseudomonas aeruginosa (PA14)[48] shaking culture supernatant was used to measure pyocyanin production over time. Planktonic cultures of PA14 were prepared by inoculation of one colony from agar plate into a 5ml lysogeny broth (Fischer Scientific) overnight. 50 µl from the 5 ml culture was diluted into 24 ml of 10 g/L tryptone media (Bactotyptone). 2 ml aliquots were made from the 24 ml tryptone media and optical density was measured every hour and the supernatant of 2 ml PA culture was collected to measure pyocyanin levels. Supernatant samples were centrifuged at 10,000 g for 20 minutes and then eluted through 0.2 micron syringe filters to remove PA cells. The rate of pyocyanin production was then used to determine the phase of PA growth.

2.4 Raman Spectroscopy

Surface enhanced Raman scattering (SERS) measurements were conducted using a Renishaw Micro Raman system with laser excitation wavelengths of 785 nm and integration time of 10 s. A laser power of 50 µW was used for all Raman and SERS measurements. The objective used for collection of SERS measurements was a 60X water immersion objective with a 1.2 NA that was wetted with DI water. The objective used for collection of pure analyte samples in cuvettes was a long range 5x objective with an NA of 0.12. In order to estimate signal enhancements due to the presence of nanosphere clusters, samples were immersed in a 10^{-3} M solution of benzenethiol (BZT) in isopropanol

for 12 hrs, followed by a methanol rinse to leave a molecular monolayer of BZT on the Au nanospheres. Enhancement factors (EF) were calculated using the following equation:[29,32,46]

$$EF = \frac{I_{SERS} / N_{SERS}}{I_{neat} / N_{neat}} \quad (1)$$

I_{SERS}, I_{neat}, N_{SERS}, N_{neat} are the SERS and neat Raman intensities, and the number of molecules for each measurement, respectively. The EF is simply the ratio of observed Raman scattering intensity of SERS measurements compared to the Raman scattering intensity of pure analyte normalized by the ratio of molecules that the spot illuminates in each case. The number of molecules measured for N_{SERS} was estimated by normalizing the area excited in the laser spot size by the BZT coverage on Au nanospheres, where

$$N_{SERS} = \rho_{surf} N_A \times 4 f_{Au} A_{Spot} \quad (2)$$

The BZT monolayer density on the Au nanospheres, ρ_{surf} is reported to be .54 nmol/cm^2 [49] and Avogadro's number, N_A, converts the molarity to a molecular density. A_{spot} is the area of the FWHM spot from a diffraction limited Gaussian beam. The fraction areal coverage of Au nanosphere, f_{Au}, is included to account for the presence of BZT only on Au regions where the cross sectional area of Au nanospheres is determined from SEM imaging; the factor of 4 is included to convert cross sectional area of a sphere to surface area as these are not 2-dimensional structures. The FWHM beam waist, w_0, used for calculating A_{spot} is obtained using the classic optics expression determining the diffraction limited beam waist as:

$$w_0 \approx \frac{\lambda_0}{\pi \times NA} \frac{\sqrt{\ln 2}}{\sqrt{2}} \quad (3)$$

Where λ_0 is the free space wavelength and the square root term converts from e^{-2} beam waist to the FWHM beam waist. Finally the FWHM spot area is calculated simply as the area of a circle with diameter w_0:

$$A_{Spot} = \frac{\pi \times w_0^2}{4} \quad (4)$$

In order to determine the number of molecules in the neat Raman measurements, the number of molecules probed from BZT solution in a cuvette is:

$$N_{Neat} = \rho_{neat} \times N_A \times V \quad (5)$$

Where ρ_{neat} is the density of benzenethiol, 9.739 mmol/cm^3 and V is the confocal volume, which is determined for the Gaussian, diffraction-limited case as:

$$V = \frac{2.33 \pi^{\frac{3}{2}} \times n}{NA} \times \frac{w_0^3}{8} \quad (6)$$

Where n is the refraction index of benzenethiol.[50] These calculations for the enhancement factor allow one to compare SERS sensor performance with other systems as it is a standard method. Yet limits in accuracy of calculated EF arise from the difference between the actual beam waist and theoretical beam waist, as the EF is proportional to volume area ratio so EF ~ w_0. If w_0 is underestimated, thereby underestimating the true interaction area, then the calculated EF will underestimate the actual enhancement; if it is overestimated the opposite will occur. While EF is only accurate with approximately an order of magnitude, the uniformity of how this is performed in the literature allows one to compare different fabricated systems with one other.

SERS spectroscopy was also performed on gradients of synthetic pyocyanin that were prepared at concentrations of 48nM, 240nM, 480nM, 2.4 μM, 4.8 μM, 9.6 μM, 19.2 μM, 28.8 μM, 38.4 μM, and 48 μM to establish the limit of detection. SERS spectroscopy was performed using the same laser power, integration times, and objective outlined above. The measurements were taken from low to high concentration with a thorough 90 s isopropanol wash of the sensor and air dried between measurements. In addition, SERS measurements were performed in the same fashion on supernatant obtained from PA14 culture as a function of incubation time. The supernatant was diluted 100:1 in deionized water and sensor surfaces were rinsed with isopropanol in between measurements as well.

3. RESULTS AND DISCUSSION

Chemical assembly of Au nanospheres is performed on poly(styrene-*b*-methyl methacrylate) (PS-*b*-PMMA) diblock copolymer templates on Si(001) substrates to form clusters with regions of high localized electric fields, referred

to as hotspots. Previous work has shown that these discrete clusters provide larger electric field enhancements, $|\vec{E}|$ than hexagonally close packed arrays,[46,51] relative to the field strength in the absence of nanostructures, $\left|\vec{E}_0\right|$; surface enhanced Raman scattering (SERS) signal enhancements scale approximately as $|\vec{E}|^4$ and thus small increases in local field strength will lead to large increases in SERS signal. PS-*b*-PMMA serves as a self-organized template to direct cluster formation on surfaces as nanospheres can selectively bind to PMMA versus PS regions.[45–47] Fig. 1 (a) depicts the chemical assembly process to deposit Au nanospheres from colloidal solution into clusters on PS-b-PMMA templates. Lipoic acid functonalized Au nanospheres having a diameter of 40 nm are assembled on templates using EDC/S-NHS crosslinking chemistry that is used to covalently attach the carboxyl groups on the nanospheres with the amine groups on the ethylenediamine functionalized PMMA regions. The nanospheres are driven to PS-b-PMMA templates using electrophoresis as shown in Fig. 1 (b). Previous work showed that electrophoretic deposition (EPD) produces high coverage of nanosphere clusters with inter-particle separation, gap spacing, on the order of 1 nm over large areas on time scales of several minutes. In comparison allowing nanospheres to diffuse to the surface via Brownian motion leads to a wider distribution of gap spacing in clusters ranging from 2-7 nm.[47] Few methods can achieve gap spacings that are less than 5 nm. For example, the electron beam in a scanning transmission electron microscope (TEM) has been used to manipulate Ag nanospheres to reach 7 nm to sub-nanometer gap spacing.[38] While TEM imaging with electron energy loss spectroscopy is interesting to experimentally measure plasmon dynamics as a function of geometry and environment,[37–39] it is impractical for large area sensor fabrication. Scholl et al. observed that gap spacings larger than 0.5 nm did not exhibit decreased dipolar resonance intensity due to quantum tunneling.[38] Thus one would expect extraordinarily large enhancement factors of Raman scattering on surfaces with nanospheres containing nanometer gap spacing as local fields can increase significantly as gap spacing decreasing to values less than 10 nm.[52] In this work, EPD was performed in two separate time periods of 10 minutes; in the first deposition period the EDC/S-NHS concentration was double than that in the second period in order to produce clusters of nanospheres quickly. These 'seed' clusters produce electrohydrodynamic flow,[53] which, in the second EPD period, promotes the formation of small clusters adjacent to the seed clusters that is designed to increase cluster density.[54] A high density of clusters is expected to lead to high SERS signal as it leads to a large number of hotspots on the surface, allowing for extremely low laser excitation intensity. Furthermore, it is particularly important at low sample volumes, μL, to have a high density of hot spots in order to minimize the amount of time for the analyte to diffuse to a hotspot for detection.

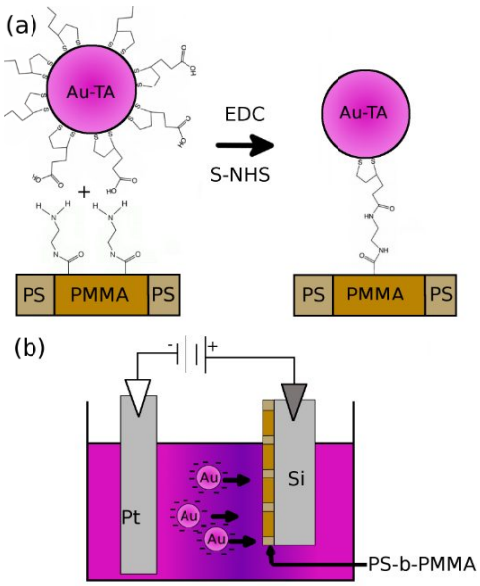

Figure 1. Schematic showing chemical assembly of Au nanospheres on self-organized PS-b-PMMA diblock copolymer templates. (a) Lipoic acid functionalized Au nanospheres having a diameter of 40 nm are covalently attached to ED-functionalized PMMA regions using EDC/S-NHS linking chemistry. (b) Au nanospheres are driven to the surface of the template serving as the working electrode with a direct current electric field.

In order to calculate an enhancement factor (EF) from SERS measurements, one must determine the coverage of Au nanospheres on the surface. Scanning electron microscopy (SEM) images were acquired after chemical assembly of lipoic acid functionalized Au nanospheres to PS-b-PMMA templates, using a Magellan XHR SEM (FEI). Assemblies of ad hoc clusters are observed in Fig. 2 (a). The PS-b-PMMA domain morphology strongly dictates cluster geometry due to the preferential attachment to the hydrophobic/hydrophilic interface between the PMMA and the PS.[47] An atomic force microscopy (AFM) topography image with line profile is shown as an inset in the right of Fig. 2 (a). The AFM image and line profile shows that the PMMA domains recede due to the ethylenediamine functionalization of this region. Lamellar domains were chosen to promote linear clusters and Fig. 2 (a) shows that the majority of the clusters conform to a quasilinear geometry. Linear clusters provide a larger local electric field enhancement in the gaps between nanospheres than circular clusters of the same size when excited with light polarized along the long axis of the cluster.[47] Analysis of the number of particles per cluster in Fig. 2 (b) shows that 85% of clusters have fewer than 5 particles. This was achieved by carefully controlling the amount of EDC/S-NHS added during chemical attachment to the surface. When larger cluster aggregates form, the electric field enhancement will approach that of an infinite hexagonally close packed lattice that is broader and less intense than discrete clusters,[43] thus this is not desirable for optimized sensor performance. A packing fraction of 0.24 was achieved that is close to the areal coverage of PMMA domains on the surface and it is also much greater than previously obtained when only a single concentration of EDC/S-NHS was used.[47] While the packing fraction is normalized in EF calculations it is still an important parameter since increasing the surface area of hotspots will increase the amount of molecules participating in SERS events and thus will improve SERS intensity, and thereby detection limit. Though as noted, when packing density reaches the HCP limit, the SERS signal will decrease again.

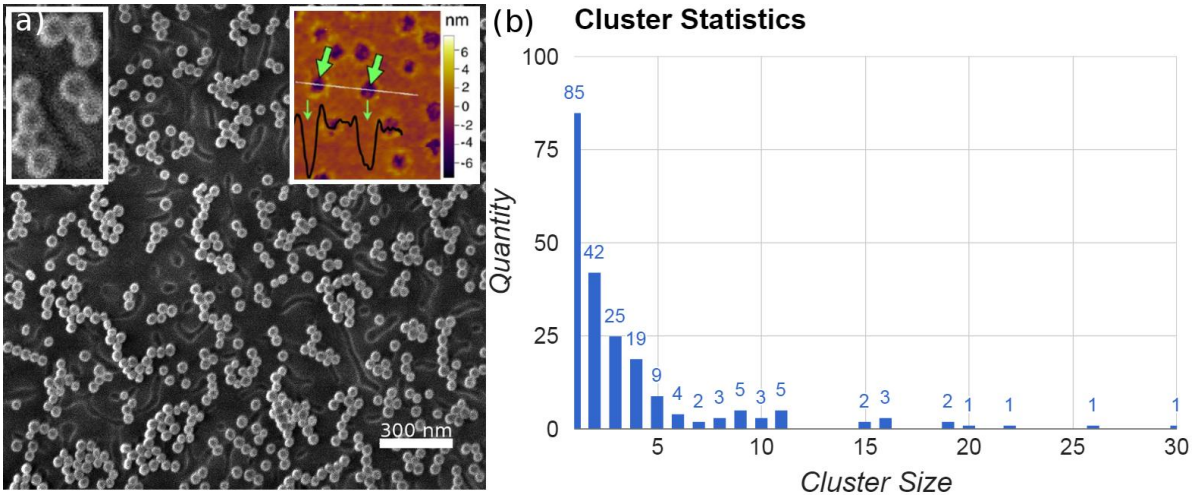

Figure 2. (a) SEM image of Au nanospheres on PS-b-PMMA templates with higher resolution inset on the left and AFM topography image with line profile is shown as an inset on the upper right. (b) Statistics of the number of clusters of a given particle number.

Experimental investigation of the electric field enhancements provided by the fabricated SERS substrates was achieved using, a well-characterized analyte, benzenethiol (BZT), as a standard. BZT forms a molecular monolayer on Au due to the strong Au-sulfur interaction[55] and thus one can calculate the number of molecules probed by the laser. BZT also has a large Raman scattering cross section[56] making it an ideal molecule for determining the performance of SERS sensors as a Raman signal is observable for pure (neat) BZT that is used as a reference to calculate enhancement of signals due to the SERS substrate.[29,32,46] Fig. 3 shows the Raman and SERS spectra of neat BZT and the SERS substrate after BZT exposure, respectively. The SERS BZT spectrum is offset by 35×10^3, and the neat spectrum is multiplied by 10 so that the Raman peaks can be observed on the same scale as the SERS measurement. The neat spectrum was acquired with a 5x objective with a NA of 0.12, while the SERS spectrum was acquired with a 60x water immersion objective whetted with DI water and with a NA of 1.2, both spectra were taken with a 50 μW and integrated

for 10s. Consider that the SERS spectra in Fig. 3 (a) is obtained from only a monolayer of BZT on the Au nanospheres with a smaller spot size while the neat BZT spectra was obtained from a pure liquid phase analyte over the entire scattering volume of the laser, so the total number of molecules illuminated by the laser is much greater for the neat BZT case. Based on the scattering volume and spot sized calculated from the FWHM beam there are approximately 5.9×10^{11} and 3.7×10^{4} molecules participating in the neat and SERS measurements, respectively. SERS spectra in Fig. 3 clearly shows significantly greater Raman scattering intensity is obtained from the SERS sensor compared with the neat BZT despite the much smaller number of molecules available to participate in Raman scattering.

Using the SERS and Raman spectra of Fig. 3 and the Au nanosphere coverage in Fig. 2, the EF was then determined as outlined in the methods section for the following characteristic BZT vibrational modes, 998 cm^{-1}, 1071 cm^{-1}, 1571 cm^{-1}. EF range from 3×10^{8} to 8×10^{9} where the vibrational mode probed leads to the largest variation in response. EF vary for different vibrational modes for several reasons, including differences in vibrational modes between the pure molecule and the metal-molecular complex and resonant enhancement due to charge-transfer transitions.[57] To explore chip-to-chip variation, EF factors for measurements using two different sensors are shown in Table 1. In previous work, SERS sensors with a reported EF of 10^{7} demonstrated a limit of detection (LOD) of arsenic at 10 parts per billion (ppb),[40] paraoxon at 275 parts per trillion (ppt),[41] and a sensor with a reported EF of 4.4×10^{8} had demonstrated LOD of 3 ppb[42] for polychlorinated biphenol. While these LOD heavily depend on both the molecule (ie. the Raman cross section of the molecule), and on the experimental set-up (ie. the laser spot size and power) the detection of these molecules at these low LOD should be achievable using the self-assembled SERS sensor fabricated in this work due to its larger EF.

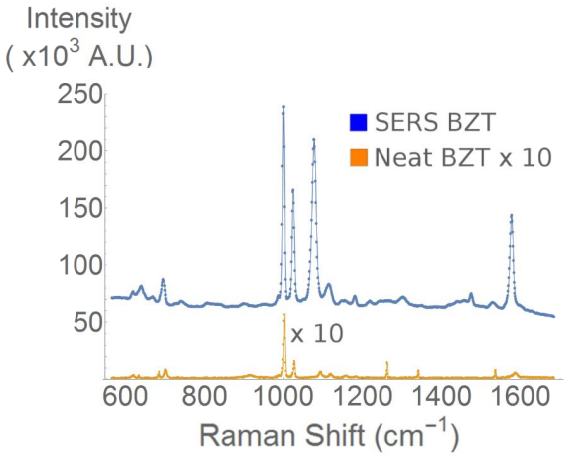

Figure 3. Measured SERS signal from benezenethiol (BZT) monolayer on Au nanospheres on PS-b-PMMA templates (blue curve) and neat Raman signal from benzenethiol solution (orange curve).

Table 1. Enhancement factors for various BZT vibrations taken from different sensors.

Vibrational frequency	Vibrational assignment	EF for sensor 1	EF for sensor 2
998 cm^{-1}	Ring out-of plane deformation and C-C symmetric stretching	5×10^{8}	3×10^{8}
1071 cm^{-1}	C-C symmetric stretching and C-S stretching	3×10^{9}	3×10^{9}
1571 cm^{-1}	C-C symmetric stretching	8×10^{9}	6×10^{9}

During functionalization of PMMA domains with amine groups using ethylenediamine, the PMMA domains appear to be etched in atomic force microscopy (AFM) images.[47] From AFM topography images, see inset of Fig. 2 (a), one can see the PMMA regions are lower than PS regions and a ridge forms around PMMA domains as PMMA is displaced; PMMA cannot be completely removed due to covalent bond between PMMA and PS in the diblock copolymer. Overall this leads to the Au nanosphere clusters to be slightly embedded in the polymer template. Previous simulations of 20nm Au clusters with gap spacing of 2 nm on PS-b-PMMA templates predicted the LSPR wavelength of nanospheres is 600 nm when the nanospheres are embedded in a dielectric environment of PMMA and analyte.[51] This value of LSPR wavelength is consistent with high SERS EF experimentally observed for 20nm Au clusters on PS-b-PMMA templates when excited at 633 nm.[46]

The higher local permittivity that results when nanospheres are embedded in the polymer template leads to a redshift of the LSPR frequency when compared to the predicted resonance frequencies for clusters in a permittivity environment of free space. In order to simulate the experimental conditions of clusters fabricated here, a multilayer structure composed of a silicon substrate, a thin film of PS-b-PMMA with average permittivity of 2.47 and thickness of 40 nm with vacuum above is illustrated in Fig. 4. Two Au nanospheres with diameter of 40 nm are partially embedded into PMMA domain. Two cases were simulated. They are referred to as Case A and Case B where 70% and 20% of dimer are embedded into the PMMA and analyte layer, respectively. The gap spacing was also varied from 1 to 2 nm. The structure was illuminated by a plane wave that is polarized along the axis of the dimer (*x* axis). We performed full-wave simulations employing the finite element method (FEM), implemented in CST Microwave Studio by Computer Simulation Technology AG. In order to find the field enhancement, we calculate $|\vec{E}|$ that is is the electric field magnitude at the center of the gold dimer relative to the electric field magnitude at the same location in the absence of dimer nanoantenna. The simulation results of $|\vec{E}|$ that shows the LSPR wavelength as the peak value are shown in Fig. 4 (b-c), where one can observe that the field enhancement and resonance wavelength are highly dependent on geometry. First by decreasing the gap from 2 nm to 1 nm, the resonance wavelength shifts to higher wavelength, redshifts, and a stronger field enhancement is obtained as expected.[47] Also, in Case A where the hot spot (gap center) is located inside the PS-b-PMMA and analyte, the field enhancement is much stronger than Case B. This result shows that dielectric medium plays an important role in designing spectroscopy systems.

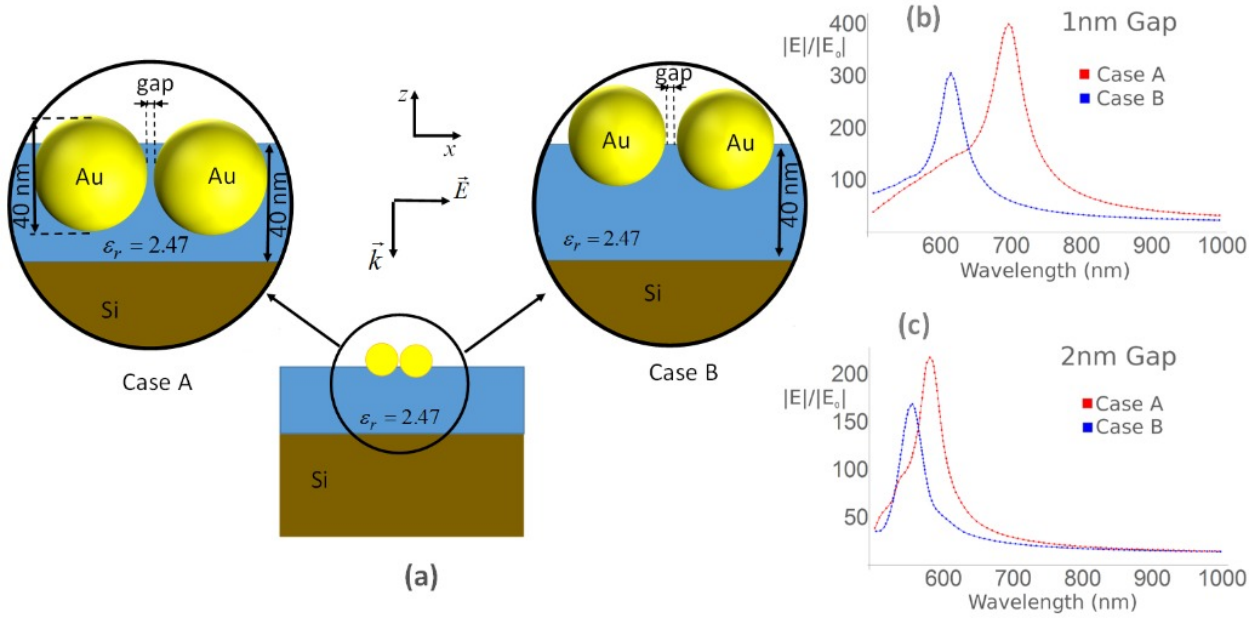

Figure 4. (a) Schematic of the simulation geometry used for the case of 70% embedded Au nanospheres (case A) and 20% embedded Au nanospheres (case B). (b) (c) Simulations of electric field enhancement in the hot spot between the nanospheres in case A and B shown for different gap spacings.

Full wave simulations for Case A with a gap distance of 1 nm show a LSPR at a wavelength of 696 nm whereas Case B has a resonance wavelength of 580 nm. When the gap is 2 nm, the LSPR is blue shifted from these values for both cases. The calculated value of $|\vec{E}|$ for Case A with a 1nm gap between nanospheres is 402, and can be used to infer a theoretical enhancement factor in SERS measurements. An enhancement of 402 yields a theoretical EF, $|\vec{E}|^4$, of 2.6×10^{10} when excited at resonance. In SERS measurements, acquired at 785 nm excitation, we calculated an EF of 6×10^9 to 8×10^9 for the C-C symmetric stretching mode. The high EF observed experimentally is consistent with Case A with 1 nm gap spacing as the structure is not excited at resonance. Indeed Fig. 3 (a) shows that the gap spacing of the 40 nm particles cannot be resolved by SEM where we typically resolved 2 nm gap spacings. As discussed earlier, previous work using the chemically assembly process described here[51] has determined that the 20 nm Au particles embedded in PMMA domain and analyte dielectric environment with a gap spacing of 2 nm had a simulated LSPR consistent with experimental observations.[47] Other work[51] has also shown that clusters with more constituent nanospheres have a LSPR that redshifts with greater electric field enhancement as the number of nanospheres in the cluster increases. In addition, the biomolecule detection studies discussed below use a water immersion objective whicalso redshift the resonance. Due to these factors a 785 nm laser was chosen to maximize the electric field enhancement for all experiments performed in this work.

SERS spectra of the quorum sensing molecule pyocyanin were acquired using 785 nm excitation through a water objective at a laser power of 50 μW and integration time of 10s. These spectra were obtained for concentrations of pyocyanin in deionized (DI) at levels between 1 part per billion (ppb) to 1 part per million (ppm) (48 nM to 48 μM). Fig. 5 (a) plots these spectra offset from each other for clarity. From this data one can observe that the most interacting vibrational peaks associated with pyocyanin appear at 636 cm^{-1}, 820 cm^{-1}, 1151 cm^{-1}, and 1567 cm^{-1}. The limit of detection (LOD) is experimentally determined to be 10 ppb from this dataset. Note the very low laser power used to perform the measurements. While some obvious signs of pyocyanin vibrational spectra are apparent in the 1 ppb and 5 ppb concentration solutions, the vibrational spectrum of the sensor prevents the determination of the existence of pyocyanin with good confidence. Examination of the SERS spectra of DI water alone reveals that the sensor substrate exhibits a complex background. These observed molecular vibrations are attributed to the linking molecule between the Au nanospheres and the nearby PS-b-PMMA.

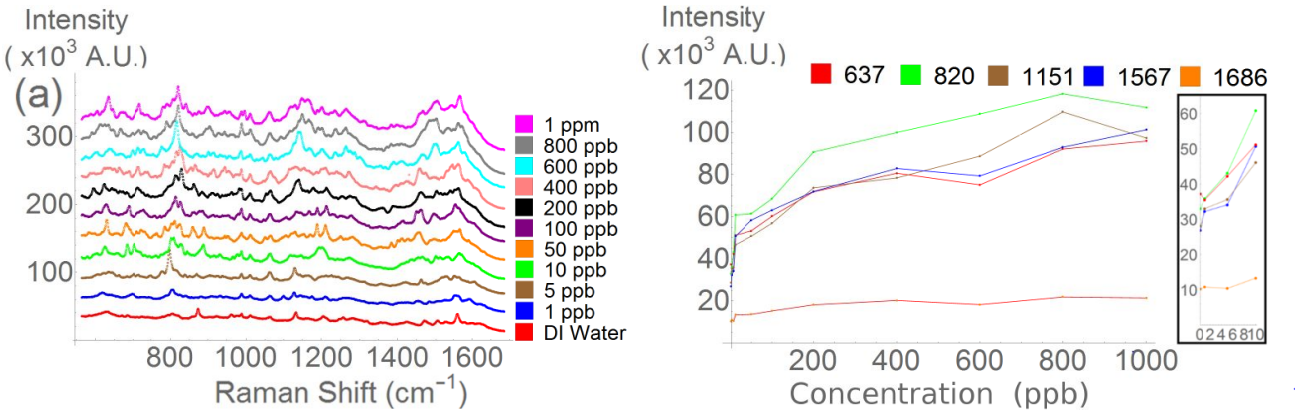

Figure 5. (a) SERS spectra for varied pyocyanin concentration in DI water. (b) Raman intensity of pyocyanin's characteristic vibrational peaks for varied pyocyanin concentration in DI water. Inset: expanded view of intensity at low concentrations.

The variation of Raman intensity with pyocyanin concentration for the characteristic vibrational peaks is plotted in Fig. 5 (b). This data shows a behavior consistent with the Langmuir molecular adsorption model, with a linear dependence of intensity on concentration at low concentrations and asymptotic behavior at large concentrations.[44] Comparison of these pyocyanin peaks to the measured intensity at 1686 cm^{-1} frequency (background) which is not associated with a pyocyanin vibrational mode for Raman scattering reveals an obvious trend that can provide rough quantitative information on the pyocyanin concentration. Slight variations in Raman intensity occur due to variations

in cluster density and particle number as the sensor is moved slightly between measurements and account for much of the slight nonlinearity in the data in Fig. 5 (b).

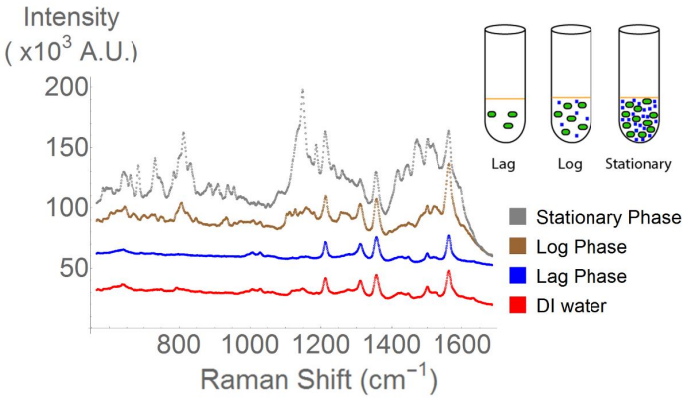

Figure 6. SERS spectra of dilute supernatant taken from *Pseudomonas aeruginosa* at various stages of their growth. Inset: schematic of pyocyanin production at the different phases of cell growth.

PA planktonic culture growth was used as a proxy for infection-associated PA biofilm growth. These cultures were sampled hourly after inoculation and measured with a spectrophotometer for optical density at 600 nm to assess cell density. Pyocyanin production is linked to cell density[18] and was used to determine the cell growth phase. Batch PA growth in shaking flasks is characterized by four major growth phases: the lag phase, the exponential growth (log) phase, the stationary phase, and the death phase. As a terminal signaling factor, pyocyanin is produced in small quantities until onset of the log phase. For this study, the spectrophotometer data was used to determine the phase of cell growth that the culture was in when the supernatant was extracted. Fig. 6 depicts the SERS spectra of the 100:1 diluted supernatant from PA cell culture at the different stages of PA growth. These spectra are offset for clarity and were obtained using the same operating parameters described above for the pure pyocyanin. The pyocyanin washes out the Raman signal from any other molecules in the PA supernatant, making SERS spectroscopy a useful tool for tracking pseudomonas growth, even without the use of antibodies or aptamers as receptor molecules. Comparison of the PA supernatant spectra in Fig. 6 with the pure pyocyanin spectra in Fig. 5 shows the presence of the pyocyanin characteristic vibrations at 636 cm^{-1}, 820 cm^{-1}, 1151 cm^{-1}, and 1567 cm^{-1}. The ability to distinguish bacterial supernatant at different stages of growth with pyocyanin is useful as a proxy for PA biofilm development. While a spectrophotometer can be used to measure cell density at high concentrations, clinical samples do not produce pyocyanin in equally large quantities as these shaken cultures, and the spectrophotometer is not selective enough for medical diagnostic use. These experiments demonstrate that the sensors developed for this work are capable biomolecule sensors.

4. CONCLUSION

In this work, the efficacy of our chemically assembled surface enhanced Raman scattering (SERS) sensors were investigated for detecting pyocyanin as a signaling agent in biofilm formation. Electrophoretic deposition of Au nanopheres using EDC/S-NHS crosslinking chemistry was observed to yield densely packed clusters over several microns in scanning electron microscopy images with gap spacings between nanospheres on the order of one nanometer. Based on the observed cluster geometry in SEM images, full wave simulations to determine the localized surface plasmon resonance conditions of the clusters and the effect of local dielectric environment of nanospheres were performed. This aided in determining most optimal commercial laser wavelength for SERS spectroscopy measurements. The Raman scattering intensity enhancement factor was then determined for comparison with other SERS platforms. This was achieved through the comparison of the Raman scattering of pure benzenethiol with molecular monolayer of benzenethiol assembled onto the sensors. The calculated enhancement factor in benzenethiol SERS measurements reached values of 8×10^9 when excited at 785 nm. Full wave simulations predict a LSPR wavelength of 700 nm and enhancement factor of 2.6×10^{10} when excited at resonance. SERS measurements at 785 nm excitation and 50 μW

power yielded a limit of detection of 10 parts per billion of pyocyanin in deionized water that was determined by tracking the linear relationship between the Raman intensity at characteristic pyocyanin molecular vibrations and the concentration of pyocyanin. Note that these are acquired with very low laser power; furthermore exciting at resonance can yield a lower limit of detection. These "molecular fingerprints," the characteristic pyocyanin molecular vibrations, were then used to determine the growth phase of a *Pseudomonas aeruginosa* (PA) culture. The work described here is a first step in using the ultrasensitive detection method to examine clinical respiratory samples obtained by patients infected with PA. Since SERS sensors do not require receptor molecules, quorum sensing molecules can also be monitored during biofilm formation to build a better understanding of quorum sensing and how to combat the biofilm formation process.

ACKNOWLEDGMENTS

The authors acknowledge the National Science Foundation NSF-EECS-1449397 and NSF-CMMI-1360060 for funding this work. We thank Dr. Dmitry Fishman of the Laser Spectroscopy Facility, University of California Irvine for his advice, and the use of his facilities. The Authors acknowledge the Laboratory for Electron and X-Ray Instrumentation (LEXI) for use of their facilities. The Authors also thank Computer Simulation Technology AG for providing CST Microwave Studio.

REFERENCES

[1] "NIH Guide: RESEARCH ON MICROBIAL BIOFILMS.", <http://grants.nih.gov/grants/guide/pa-files/PA-03-047.html> (13 August 2015).
[2] Revdiwala, S., Rajdev, B. M.., Mulla, S., "Characterization of Bacterial Etiologic Agents of Biofilm Formation in Medical Devices in Critical Care Setup," Crit. Care Res. Pract. **2012**, e945805 (2012).
[3] Stewart, P. S.., William Costerton, J., "Antibiotic resistance of bacteria in biofilms," The Lancet **358**(9276), 135–138 (2001).
[4] Kolter, R.., Greenberg, E. P., "Microbial sciences: The superficial life of microbes," Nature **441**(7091), 300–302 (2006).
[5] Soto, S. M., "Role of efflux pumps in the antibiotic resistance of bacteria embedded in a biofilm," Virulence **4**(3), 223–229 (2013).
[6] Elliott, T. S., Moss, H. A., Tebbs, S. E., Wilson, I. C., Bonser, R. S., Graham, T. R., Burke, L. P.., Faroqui, M. H., "Novel approach to investigate a source of microbial contamination of central venous catheters," Eur. J. Clin. Microbiol. Infect. Dis. Off. Publ. Eur. Soc. Clin. Microbiol. **16**(3), 210–213 (1997).
[7] Garland, A. L., Walton, W. G., Coakley, R. D., Tan, C. D., Gilmore, R. C., Hobbs, C. A., Tripathy, A., Clunes, L. A., Bencharit, S., et al., "Molecular basis for pH-dependent mucosal dehydration in cystic fibrosis airways," Proc. Natl. Acad. Sci. **110**(40), 15973–15978 (2013).
[8] Cheng, S. H., Gregory, R. J., Marshall, J., Paul, S., Souza, D. W., White, G. A., O'Riordan, C. R.., Smith, A. E., "Defective intracellular transport and processing of CFTR is the molecular basis of most cystic fibrosis," Cell **63**(4), 827–834 (1990).
[9] Ulrich, M., Worlitzsch, D., Viglio, S., Siegmann, N., Iadarola, P., Shute, J. K., Geiser, M., Pier, G. B., Friedel, G., et al., "Alveolar inflammation in cystic fibrosis," J. Cyst. Fibros. **9**(3), 217–227 (2010).
[10] Bjarnsholt, T., Jensen, P. Ø., Fiandaca, M. J., Pedersen, J., Hansen, C. R., Andersen, C. B., Pressler, T., Givskov, M.., Høiby, N., "Pseudomonas aeruginosa biofilms in the respiratory tract of cystic fibrosis patients," Pediatr. Pulmonol. **44**(6), 547–558 (2009).
[11] Høiby, N., Frederiksen, B.., Pressler, T., "Eradication of early Pseudomonas aeruginosa infection," J. Cyst. Fibros. **4, Supplement 2**, 49–54 (2005).
[12] Folkesson, A., Jelsbak. L., Yang, L., Johansen, H.K., Ciofu, O., Høiby, N., Molin, S. "Adaptation of Pseudomonas aeruginosa to the cystic fibrosis airway: an evolutionary perspective" Nat. Rev. Microbiol. **10**, 841-851 (2012).
[13] Burns, J. L., Gibson, R. L., McNamara, S., Yim, D., Emerson, J., Rosenfeld, M., Hiatt, P., McCoy, K., Castile, R., et al., "Longitudinal Assessment of Pseudomonas aeruginosa in Young Children with Cystic Fibrosis," J. Infect. Dis. **183**(3), 444–452 (2001).

[14] Lister, P. D., Wolter, D. J.., Hanson, N. D., "Antibacterial-Resistant Pseudomonas aeruginosa: Clinical Impact and Complex Regulation of Chromosomally Encoded Resistance Mechanisms," Clin. Microbiol. Rev. **22**(4), 582–610 (2009).
[15] Singh, P. K., Schaefer, A. L., Parsek, M. R., Moninger, T. O., Welsh, M. J.., Greenberg, E. P., "Quorum-sensing signals indicate that cystic fibrosis lungs are infected with bacterial biofilms," Nature **407**(6805), 762–764 (2000).
[16] Kievit, T. R. D., Gillis, R., Marx, S., Brown, C.., Iglewski, B. H., "Quorum-Sensing Genes in Pseudomonas aeruginosa Biofilms: Their Role and Expression Patterns," Appl. Environ. Microbiol. **67**(4), 1865–1873 (2001).
[17] Miller, M. B.., Bassler, B. L., "Quorum Sensing in Bacteria," Annu. Rev. Microbiol. **55**(1), 165–199 (2001).
[18] Lau, G. W., Hassett, D. J., Ran, H.., Kong, F., "The role of pyocyanin in Pseudomonas aeruginosa infection," Trends Mol. Med. **10**(12), 599–606 (2004).
[19] Davies, J. C., "Pseudomonas aeruginosa in cystic fibrosis: pathogenesis and persistence," Paediatr. Respir. Rev. **3**(2), 128–134 (2002).
[20] Glasser, N. R., Kern, S. E.., Newman, D. K., "Phenazine redox cycling enhances anaerobic survival in Pseudomonas aeruginosa by facilitating generation of ATP and a proton-motive force," Mol. Microbiol. **92**(2), 399–412 (2014).
[21] Hunter, R. C., Klepac-Ceraj, V., Lorenzi, M. M., Grotzinger, H., Martin, T. R.., Newman, D. K., "Phenazine content in the cystic fibrosis respiratory tract negatively correlates with lung function and microbial complexity," Am. J. Respir. Cell Mol. Biol. **47**(6), 738–745 (2012).
[22] Brolo, A. G., "Plasmonics for future biosensors," Nat. Photonics **6**(11), 709–713 (2012).
[23] Novotny, L.., Hecht, B., Principles of Nano-Optics, Cambridge University Press (2012).
[24] Boyd, R. W., Nonlinear Optics, Academic Press (2003).
[25] Nie, S.., Emory, S. R., "Probing Single Molecules and Single Nanoparticles by Surface-Enhanced Raman Scattering," Science **275**(5303), 1102–1106 (1997).
[26] Kneipp, K., Wang, Y., Kneipp, H., Perelman, L. T., Itzkan, I., Dasari, R. R.., Feld, M. S., "Single Molecule Detection Using Surface-Enhanced Raman Scattering (SERS)," Phys. Rev. Lett. **78**(9), 1667–1670 (1997).
[27] Maier, S. A., Plasmonics: Fundamentals and Applications, Springer Science & Business Media (2007).
[28] Kerker, M., Wang, D.-S.., Chew, H., "Surface enhanced Raman scattering (SERS) by molecules adsorbed at spherical particles," Appl. Opt. **19**(19), 3373 (1980).
[29] Fleischmann, M., Hendra, P. J.., McQuillan, A. J., "Raman spectra of pyridine adsorbed at a silver electrode," Chem. Phys. Lett. **26**(2), 163–166 (1974).
[30] Busby, C. C.., Creighton, J. A., "Efficient gold and silver electrodes for surface enchanced raman spectral studies of electrochemical systems: The behaviour of pyridine and naphthalene adsorbed on roughened gold electrodes," J. Electroanal. Chem. Interfacial Electrochem. **140**(2), 379–390 (1982).
[31] Sharac, N., Sharma, H., Khine, M.., Ragan, R., "Tunable nano bead arrays on film for controlling propogation of light," Proc. SPIE, **8809**, 88091O – 8 (2013).
[32] Caldwell, J. D., Glembocki, O., Bezares, F. J., Bassim, N. D., Rendell, R. W., Feygelson, M., Ukaegbu, M., Kasica, R., Shirey, L., et al., "Plasmonic Nanopillar Arrays for Large-Area, High-Enhancement Surface-Enhanced Raman Scattering Sensors," ACS Nano **5**(5), 4046–4055 (2011).
[33] Schuck, P. J., Fromm, D. P., Sundaramurthy, A., Kino, G. S.., Moerner, W. E., "Improving the Mismatch between Light and Nanoscale Objects with Gold Bowtie Nanoantennas," Phys. Rev. Lett. **94**(1), 017402 (2005).
[34] Kinkhabwala, A. A., Coupling Fluorophores Molecules to Nanophotonic Structures, Stanford University (2010).
[35] Vieu, C., Carcenac, F., Pépin, A., Chen, Y., Mejias, M., Lebib, A., Manin-Ferlazzo, L., Couraud, L.., Launois, H., "Electron beam lithography: resolution limits and applications," Appl. Surf. Sci. **164**(1–4), 111–117 (2000).
[36] Melngailis, J., "Focused ion beam lithography," Nucl. Instrum. Methods Phys. Res. Sect. B Beam Interact. Mater. At. **80–81, Part 2**, 1271–1280 (1993).
[37] Koh, A. L., Bao, K., Khan, I., Smith, W. E., Kothleitner, G., Nordlander, P., Maier, S. A.., McComb, D. W., "Electron Energy-Loss Spectroscopy (EELS) of Surface Plasmons in Single Silver Nanoparticles and Dimers: Influence of Beam Damage and Mapping of Dark Modes," ACS Nano **3**(10), 3015–3022 (2009).
[38] Scholl, J. A., García-Etxarri, A., Koh, A. L.., Dionne, J. A., "Observation of Quantum Tunneling between Two Plasmonic Nanoparticles," Nano Lett. **13**(2), 564–569 (2013).
[39] Kadkhodazadeh, S., de Lasson, J. R., Beleggia, M., Kneipp, H., Wagner, J. B.., Kneipp, K., "Scaling of the Surface Plasmon Resonance in Gold and Silver Dimers Probed by EELS," J. Phys. Chem. C **118**(10), 5478–5485 (2014).

[40] Manfrinato, V. R., Zhang, L., Su, D., Duan, H., Hobbs, R. G., Stach, E. A.., Berggren, K. K., "Resolution Limits of Electron-Beam Lithography toward the Atomic Scale," Nano Lett. **13**(4), 1555–1558 (2013).
[41] Wu, H.-Y.., Cunningham, B. T., "Point-of-care detection and real-time monitoring of intravenously delivered drugs via tubing with an integrated SERS sensor," Nanoscale **6**(10), 5162–5171 (2014).
[42] Negri, P., Choi, J. Y., Jones, C., Tompkins, S. M., Tripp, R. A.., Dluhy, R. A., "Identification of Virulence Determinants in Influenza Viruses," Anal. Chem. **86**(14), 6911–6917 (2014).
[43] Granger, J. H., Granger, M. C., Firpo, M. A., Mulvihill, S. J.., Porter, M. D., "Toward development of a surface-enhanced Raman scattering (SERS)-based cancer diagnostic immunoassay panel," The Analyst **138**(2), 410–416 (2013).
[44] Kim, A., Barcelo, S. J., Williams, R. S.., Li, Z., "Melamine Sensing in Milk Products by Using Surface Enhanced Raman Scattering," Anal. Chem. **84**(21), 9303–9309 (2012).
[45] Choi, J. H., Adams, S. M.., Ragan, R., "Design of a versatile chemical assembly method for patterning colloidal nanoparticles," Nanotechnology **20**(6), 065301 (2009).
[46] Adams, S. M., Campione, S., Caldwell, J. D., Bezares, F. J., Culbertson, J. C., Capolino, F.., Ragan, R., "Non-lithographic SERS Substrates: Tailoring Surface Chemistry for Au Nanoparticle Cluster Assembly," Small **8**(14), 2239–2249 (2012).
[47] Adams, S. M., Campione, S., Capolino, F.., Ragan, R., "Directing Cluster Formation of Au Nanoparticles from Colloidal Solution," Langmuir **29**(13), 4242–4251 (2013).
[48] Rahme, L. G., Stevens, E. J., Wolfort, S. F., Shao, J., Tompkins, R. G.., Ausubel, F. M., "Common virulence factors for bacterial pathogenicity in plants and animals," Science **268**(5219), 1899–1902 (1995).
[49] Gui, J. Y., Stern, D. A., Frank, D. G., Lu, F., Zapien, D. C.., Hubbard, A. T., "Adsorption and surface structural chemistry of thiophenol, benzyl mercaptan, and alkyl mercaptans. Comparative studies at silver(111) and platinum(111) electrodes by means of Auger spectroscopy, electron energy loss spectroscopy, low energy electron diffraction and electrochemistry," Langmuir **7**(5), 955–963 (1991).
[50] Wohlfarth, Christian., Static Dielectric Constants of Pure Liquids and Binary Liquid Mixtures | Christian Wohlfarth | Springer, Editor: O. Madelung, Springer-Verlag, Berlin (1991).
[51] Campione, S., Adams, S. M., Ragan, R.., Capolino, F., "Comparison of electric field enhancements: Linear and triangular oligomers versus hexagonal arrays of plasmonic nanospheres," Opt. Express **21**(7), 7957–7973 (2013).
[52] Romero, I., Aizpurua, J., Bryant, G. W.., García De Abajo, F. J., "Plasmons in nearly touching metallic nanoparticles: singular response in the limit of touching dimers," Opt. Express **14**(21), 9988 (2006).
[53] Nadal, F., Argoul, F., Kestener, P., Pouligny, B., Ybert, C.., Ajdari, A., "Electrically induced flows in the vicinity of a dielectric stripe on a conducting plane," Eur. Phys. J. E - Soft Matter **9**(4), 387–399 (2002).
[54] Patel, M. N., Williams, R. D., May, R. A., Uchida, H., Stevenson, K. J.., Johnston, K. P., "Electrophoretic Deposition of Au Nanocrystals inside Perpendicular Mesochannels of TiO2," Chem. Mater. **20**(19), 6029–6040 (2008).
[55] Xue, Y., Li, X., Li, H.., Zhang, W., "Quantifying thiol–gold interactions towards the efficient strength control," Nat. Commun. **5** , 4348 (2014).
[56] Aggarwal, R. L., Farrar, L. W., Diebold, E. D.., Polla, D. L., "Measurement of the absolute Raman scattering cross section of the 1584-cm−1 band of benzenethiol and the surface-enhanced Raman scattering cross section enhancement factor for femtosecond laser-nanostructured substrates," J. Raman Spectrosc. **40**(9), 1331–1333 (2009).
[57] Saikin, S. K., Olivares-Amaya, R., Rappoport, D., Stopa, M.., Aspuru-Guzik, A., "On the chemical bonding effects in the Raman response: Benzenethiol adsorbed on silver clusters," Phys. Chem. Chem. Phys. **11**(41), 9401 (2009).